symmetry

MDPI

Article

$\mathcal{P},\mathcal{T}$-Violating and Magnetic Hyperfine Interactions in Atomic Thallium

Timo Fleig [1,*] and Leonid V. Skripnikov [2]

[1] Laboratoire de Chimie et Physique Quantiques, IRSAMC, Université Paul Sabatier Toulouse III, 118 Route de Narbonne, F-31062 Toulouse, France

[2] B.P. Konstantinov Petersburg Nuclear Physics Institute of National Research Centre "Kurchatov Institute", Gatchina, 188300 Leningrad District, Russia; leonidos239@gmail.com

* Correspondence: timo.fleig@irsamc.ups-tlse.fr

Received: 5 March 2020; Accepted: 17 March 2020; Published: 30 March 2020

Abstract: We present state-of-the-art string-based relativistic general-excitation-rank configuration interaction and coupled cluster calculations of the electron electric dipole moment, the nucleon–electron scalar-pseudoscalar, and the magnetic hyperfine interaction constants ($\alpha_{d_e}, \alpha_{C_S}, A_{||}$, respectively) for the thallium atomic ground state $^2P_{1/2}$. Our present best values are $\alpha_{d_e} = -558 \pm 28$, $\alpha_{C_S} = 6.77 \pm 0.34$ [$10^{-18} e$ cm], and $A_{||} = 21172 \pm 1059$ [MHz]. The central value of the latter constant agrees with the experimental result to within 0.7% and serves as a measurable probe of the $\mathcal{P},\mathcal{T}$-violating interaction constants. Our findings lead to a significant reduction of the theoretical uncertainties for $\mathcal{P},\mathcal{T}$-odd interaction constants for atomic thallium but not to stronger constraints on the electron electric dipole moment, d_e, or the nucleon–electron scalar-pseudoscalar coupling constant, C_S.

Keywords: electron electric dipole moment; scalar-pseudoscalar interaction; magnetic hyperfine interaction; relativistic many-body theory

1. Introduction

Electric dipole moments (EDM) of elementary particles, atoms and molecules give rise to spatial parity ($\mathcal{P}$) and time-reversal ($\mathcal{T}$) violating interactions [1] and are a powerful probe for physics beyond the standard model (BSM) [2]. Current single-source limits [3–5] on the electron EDM, for instance, can probe New Physics (NP) up to an energy scale of 1000 TeV [6] (radiative stability approach) or even greater [7], surpassing the current sensitivity of the Large Hadron Collider for corresponding sources of NP.

Until today no low-energy EDM experiment has delivered a positive result. However, the obtained EDM upper bounds are useful for constraining $\mathcal{CP}$-violating parameters [8] of BSM models, cast as effective field theories [6,9] at different energy scales.

Open-shell atomic and molecular systems are particularly sensitive probes of leptonic and semi-leptonic $\mathcal{CP}$-violation [10]. In most BSM models [11] the dominant $\mathcal{CP}$-odd sources are the electron EDM, d_e, and the nucleon–electron scalar-pseudoscalar (Ne-SPS) coupling, C_S. Figure 1 (Courtesy: Martin Jung, Torino, Italy (2019)) shows the constraints (yellow surface) on d_e and C_S using the combined information from measurements [3,12–14] and calculations [4,5,15–23], including the associated experimental and theoretical uncertainties, on the open-shell systems ThO (green), YbF (red; the red surface underlies the others and its extent is indicated by the thin red line), HfF^+ (orange) and Tl (blue) through a global fit in the d_e/C_S plane. Results from a single system do, therefore, not constrain d_e or C_S individually at all in this multiple-source interpretation [24], but lead to a

fan-shaped surface of allowed combinations. The width of this surface is a function of the experimental and theoretical uncertainties.

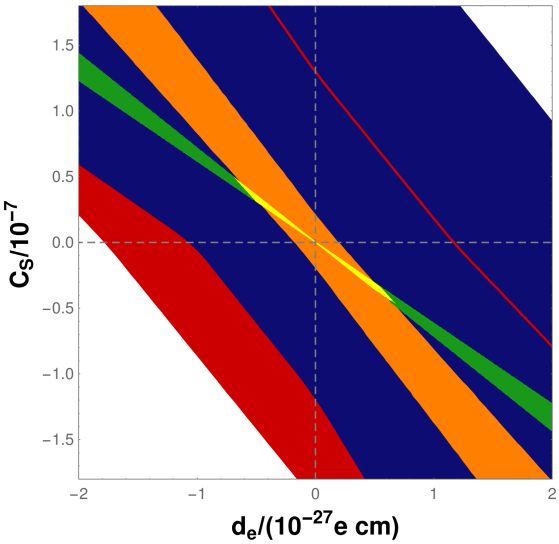

Figure 1. Constraints on d_e and C_S without the results of this work. See text for details.

This means that a substantial reduction of an uncertainty for an individual system could lead to more stringent constraints on the unknown $\mathcal{CP}$-violating parameters. The main reason for this is that the surfaces for different systems are not fully aligned, which is due to the different dependency of electron EDM and Ne-SPS atomic interactions on the electric charge of the respective heavy nuclei [25].

A substantial part of the width of the surface for the Tl atom is due to the great spread of theoretical values for the electron EDM atomic enhancement, R, calculated in the past by various groups using different electronic-structure approaches [1,19–23,26]. Strikingly, Nataraj et al. [22] used a high-level many-body approach, the Coupled Cluster (CC) method, and produced a value for R that strongly disagrees with the results from all other groups that have included electron correlation effects, on the order of 20%.

The purpose of this paper is two-fold:

1. We use state-of-the-art relativistic Configuration Interaction (CI) and Coupled Cluster approaches for large-scale applications to determine the mentioned atomic interaction constants. Our calculations represent the most elaborate treatment of electron correlation effects to date on the discussed properties of the thallium atom ground state. We put particular emphasis on the electron EDM enhancement R and a conclusive resolution of the major discrepancy between literature values. Claims about physical effects that purportedly underlie these discrepancies are scrutinized.
2. We investigate whether a reduced uncertainty for R(Tl) impacts the above-described constraints on d_e and C_S.

The paper is structured as follows. In Section 2 we lay out the theory underlying the atomic electron EDM, Ne-SPS, and magnetic hyperfine interaction constants. Electron EDM and Ne-SPS interactions are both sensitive to electron spin density in the vicinity of the atomic nucleus. The same is true for the magnetic hyperfine interaction. For this reason, the latter is an experimentally measurable probe for the New Physics atomic interaction constants (that cannot be measured by experiment), and we thus include it in our study as a validating property. The following Section 3 contains technical details about our calculations, results, and a discussion of these results in comparison with literature values. The final Section 4 concludes on our findings.

2. Theory

An atomic EDM is defined [27] (p. 16) as

$$d_a = -\lim_{E_{\text{ext}}\to 0}\left[\frac{\partial(\Delta\varepsilon)}{\partial E_{\text{ext}}}\right] \tag{1}$$

where $\Delta\varepsilon$ is a $\mathcal{P},\mathcal{T}$-odd energy shift and E_{ext} is an external electric field. In atoms with nuclear spin $I \leq \frac{1}{2}$ [28] and in an electronic state with unpaired electrons, this energy shift is dominated by and originates from either the electron EDM, d_e, or a $\mathcal{P},\mathcal{T}$-odd nucleon–electron (Ne) interaction, or a combination of the two [10,11]. The two cases are presented separately.

2.1. Atomic Edm Due to Electron Edm

The Hamiltonian for the interaction of the electron electric dipole moment, d_e, is for an atomic system

$$H_{\text{EDM}} = -\sum_j \mathbf{d}_j \cdot \mathbf{E}(\mathbf{r}_j) = -d_e \sum_j \gamma_j^0 \boldsymbol{\Sigma}_j \cdot \mathbf{E}(\mathbf{r}_j) \tag{2}$$

where γ^0 is a Dirac matrix, $\boldsymbol{\Sigma} = \begin{pmatrix} \sigma & \mathbf{0} \\ \mathbf{0} & \sigma \end{pmatrix}$ is a vector of spin matrices in Dirac representation, j is an electron index, $\mathbf{E}(\mathbf{r}_j)$ the electric field at position $\mathbf{r}_j$ and the bare fermion's electric dipole moment is expressed as $\mathbf{d} = d_e\,\gamma^0\,\boldsymbol{\Sigma}$, necessarily linearly dependent on the particle's spin vector $\boldsymbol{\Sigma}$ [1,29].

Supposing a non-zero electron EDM d_e, the resulting energy shift can be evaluated as

$$\Delta\varepsilon_{\text{EDM}} = d_e \left\langle -\sum_j \gamma_j^0 \boldsymbol{\Sigma}_j \cdot \mathbf{E}(\mathbf{r}_j) \right\rangle_{\psi(E_{\text{ext}})} \tag{3}$$

where $\psi(E_{\text{ext}})$ is the field-dependent atomic wavefunction of the state in question. The expectation value in Equation (3) has the physical dimension of electric field and can be regarded as the mean interaction of each electron EDM with this field in the respective state. Following stratagem II of Lindroth et al. [30] the expectation value is recast in electronic momentum form as an effective one-body operator

$$\left\langle -\sum_j \gamma_j^0 \boldsymbol{\Sigma}_j \cdot \mathbf{E}(\mathbf{r}_j) \right\rangle_{\psi(E_{\text{ext}})} \approx \frac{2\imath c}{e\hbar} \left\langle \sum_j \gamma_j^0 \gamma_j^5 \mathbf{p}_j^2 \right\rangle_{\psi(E_{\text{ext}})} \tag{4}$$

where the approximation lies in assuming that ψ is an exact eigenfunction of the field-dependent Hamiltonian of the system. This momentum-form EDM operator has already been used as early as in 1986, by Johnson et al. [26]. In the present work the field-dependent Hamiltonian is the Dirac-Coulomb Hamiltonian (in *a.u.*, $e = m_e = \hbar = 1$)

$$\begin{aligned} \hat{H} &:= \hat{H}^{\text{Dirac-Coulomb}} + \hat{H}^{\text{Int-Dipole}} \\ &= \sum_j^n \left[c\,\boldsymbol{\alpha}_j \cdot \mathbf{p}_j + \beta_j c^2 - \frac{Z}{r_{jK}} \mathbb{1}_4 \right] + \sum_{k>j}^n \frac{1}{r_{jk}} \mathbb{1}_4 + \sum_j \mathbf{r}_j \cdot \mathbf{E}_{\text{ext}}\, \mathbb{1}_4 \end{aligned} \tag{5}$$

with $\mathbf{E}_{\text{ext}}$ weak and homogeneous, the indices j,k run over n electrons, Z the proton number with the nucleus K placed at the origin, and $\boldsymbol{\alpha}$ are standard Dirac matrices. E_{ext} is not treated as a perturbation but included *a priori* in the variational optimization of the atomic wavefunction. Furthermore, the final results reported in this work include high excitation ranks in the correlation expansion of ψ. For these reasons, the approximation in Equation (4) is considered very good in the present case.

Within the so-defined picture and using Equations (1), (3), and (4) the atomic EDM becomes

$$d_a = -\lim_{E_{\text{ext}}\to 0} \frac{\partial}{\partial E_{\text{ext}}} \frac{2\imath c\, d_e}{e\hbar} \left\langle \sum_j \gamma_j^0 \gamma_j^5 \mathbf{p}_j^2 \right\rangle_{\psi(E_{\text{ext}})}. \tag{6}$$

The (dimensionless) atomic EDM enhancement factor is defined as $R := \frac{d_a}{d_e}$. Denoting $E_{\text{eff}} = \frac{2\imath c}{e\hbar} \left\langle \sum_j \gamma_j^0 \gamma_j^5 \mathbf{p}_j^2 \right\rangle_{\psi(E_{\text{ext}})}$ for the sake of simplicity, the enhancement factor is

$$R = -\lim_{E_{\text{ext}}\to 0} \left[\frac{\partial E_{\text{eff}}}{\partial E_{\text{ext}}} \right]. \tag{7}$$

The external field used in the experiment on Tl [14] was $E_{\text{ext}} = 1.23 \times 10^7 \left[\frac{\text{V}}{\text{m}}\right] \approx 0.2392 \times 10^{-4}$ a.u. In the present work $E_{\text{ext}} = 0.24 \times 10^{-4}$ a.u. is used. This is a very small field which is well within the linear regime considering the derivative in Equation (7). The enhancement factor may under these circumstances be written as a function of two field points

$$R_{\text{lin}} = -\frac{\Delta E_{\text{eff}}}{\Delta E_{\text{ext}}} = -\frac{E_{\text{eff}}(2) - E_{\text{eff}}(1)}{E_{\text{ext}}(2) - E_{\text{ext}}(1)}. \tag{8}$$

We set $E_{\text{ext}}(1) := 0$, in which case atomic states are parity eigenstates. Since the EDM operator is parity odd, it follows that $E_{\text{eff}}(1) = 0$, and so

$$R \approx R_{\text{lin}} = -\frac{E_{\text{eff}}}{E_{\text{ext}}}. \tag{9}$$

E_{eff} is calculated as described in reference [31]. ψ is an approximate configuration interaction (CI) eigenfunction of the Dirac-Coulomb Hamiltonian including E_{ext}. Alternatively, E_{eff} can be calculated within the finite-field approach [32,33]. The latter has been used in coupled cluster calculations.

The electron EDM enhancement factor R is in the particle physics literature often denoted as

$$\alpha_{d_e} := R, \tag{10}$$

the atomic-scale interaction constant of the electron EDM.

2.2. Nucleon–Electron Scalar-Pseudoscalar Interaction

The effective Hamiltonian for a $\mathcal{P},\mathcal{T}$-odd nucleon–electron scalar-pseudoscalar interaction is written as [34]

$$H_{\text{Ne-SPS}} = \imath \frac{G_F}{\sqrt{2}} A C_S \sum_j \gamma_j^0 \gamma_j^5 \rho_N(\mathbf{r}_j) \tag{11}$$

and the resulting atomic energy shift is accordingly

$$\Delta\varepsilon_{\text{Ne-SPS}} = \frac{G_F}{\sqrt{2}} A C_S \left\langle \imath \sum_j \gamma_j^0 \gamma_j^5 \rho_N(\mathbf{r}_j) \right\rangle_{\Psi(E_{\text{ext}})}, \tag{12}$$

where A is the nucleon number, C_S is the S-PS nucleon–electron coupling constant, G_F is the Fermi constant (A comment on units: Its value is $\frac{G_F}{(\hbar c)^3} = 1.166364 \times 10^{-5}[\text{GeV}]^{-2} = 0.86366 \times 10^{-20} E_H^{-2}$. With $\hbar = 1$ a.u. and $c = 137.036$ a.u., the Fermi constant is also expressed as $G_F = 2.2225 \times 10^{-14}$ a.u.) and $\rho_N(\mathbf{r}_j)$ is the nucleon density at the position of electron j. Please note that in the present work we define $\gamma^5 := \imath\gamma^0\gamma^1\gamma^2\gamma^3$, whereas Flambaum and co-workers [21,25] define $\gamma^5 := -\imath\gamma^0\gamma^1\gamma^2\gamma^3$ which

explains the sign difference between the present Ne-SPS atomic interaction constants and those of Flambaum and co-workers.

Next, we define (see also reference [35]) in analogy with Equation (7) an Ne-SPS ratio (The physical dimension of the S ratio is $\dim(S) = \dim\left(\frac{\rho_N}{E}\right) = \left[\frac{Q\,T^2}{M\,L^4}\right]$. This is consistent with the dimension of S in the definition, Equation (13), where $\dim(S) = \dim\left(\frac{d_a}{C_S\,G_F}\right) = \left[\frac{Q\,T^2}{M\,L^4}\right]$.)

$$S := \frac{d_a}{A C_S \frac{G_F}{\sqrt{2}}} \tag{13}$$

and so one can write, using Equation (1),

$$S = -\lim_{E_{\text{ext}}\to 0}\left[\frac{\partial}{\partial E_{\text{ext}}}\left\langle \imath \sum_j \gamma_j^0\,\gamma_j^5\,\rho_N(\mathbf{r}_j)\right\rangle_{\Psi(E_{\text{ext}})}\right] \tag{14}$$

and in the linear regime

$$S = -\frac{\left\langle \imath \sum_j \gamma_j^0\,\gamma_j^5\,\rho_N(\mathbf{r}_j)\right\rangle_{\Psi(E_{\text{ext}})}}{E_{\text{ext}}}. \tag{15}$$

The initial implementation of this expectation value in the latter expression has been described in reference [36]. The independent implementation of the matrix elements of the Hamiltonian (11) has been developed in ref. [4].

For comparison with literature results we also define the S-PS nucleon–electron interaction constant

$$\alpha_{C_S} := \frac{d_a}{C_S} = S\,A\,\frac{G_F}{\sqrt{2}}. \tag{16}$$

2.3. Magnetic Hyperfine Interaction

Minimal substitution according to $\mathbf{p} \longrightarrow \mathbf{p} - \frac{q}{c}\mathbf{A}$ in the Dirac equation and the representation of the vector potential in magnetic dipole approximation as $\mathbf{A}_D(\mathbf{r}) = \frac{\mathbf{m}\times\mathbf{r}}{r^3}$ with $\mathbf{m}$ the nuclear magnetic dipole moment leads to the magnetic hyperfine Hamiltonian

$$\hat{H}_{\text{HF}} = c\boldsymbol{\alpha}\cdot\left(-\frac{q}{c}\,\frac{\mathbf{m}\times\mathbf{r}}{r^3}\right) = q\,\mathbf{m}\cdot\left(\frac{\boldsymbol{\alpha}\times\mathbf{r}}{r^3}\right) \tag{17}$$

for a single point charge q at position $\mathbf{r}$ outside the finite nucleus. Given the nuclear magnetic dipole moment vector as $\mathbf{m} = \frac{\mu}{I}\,\mu_N\,\mathbf{I} = g_I\,\mu_N\,\mathbf{I}$ where μ is the magnetic moment in nuclear magnetons (μ_N), g_I is the nuclear g-factor, and $\mathbf{I}$ is the nuclear spin, Equation (17) for a single electron is written as

$$\hat{H}_{\text{HF}} = -e\,\frac{\mu}{I}\,\mu_N\,\mathbf{I}\cdot\left(\frac{\boldsymbol{\alpha}\times\mathbf{r}}{r^3}\right) \tag{18}$$

Based on Equation (18) we now define the magnetic hyperfine interaction constant for n electrons in the field of nucleus K (in *a.u.*)

$$A_{||}(K) = -\frac{\mu_K[\mu_N]}{2cIm_pM_J}\left\langle \Psi_{J,M_J}\middle|\sum_{i=1}^{n}\left(\frac{\boldsymbol{\alpha}_i\times\mathbf{r}_{iK}}{r_{iK}^3}\right)_z\middle|\Psi_{J,M_J}\right\rangle \tag{19}$$

where $\frac{1}{2cm_p}$ is the nuclear magneton in *a.u.*, and m_p is the proton rest mass. The term $\frac{1}{M_J}$ in the prefactor of Equation (19) is explained as follows.

The vector operator $\left(\frac{\boldsymbol{\alpha}_i \times \mathbf{r}_{iK}}{r_{iK}^3}\right)_z$ can be regarded as the $q = 0$ component of a rank $k = 1$ irreducible tensor operator $\hat{T}_q^{(k)}$. Application of the Wigner-Eckart Theorem to the diagonal matrix element in Equation (19) yields

$$\left\langle \alpha, J, M_J | \hat{T}_0^{(1)} | \alpha, J, M_J \right\rangle = \left\langle J, M_J; 1, 0 | J, 1; J, M_J \right\rangle \frac{\left\langle \alpha, J || \hat{T}^{(1)} || \alpha, J \right\rangle}{\sqrt{2J+1}}$$

where the Clebsch–Gordan coefficient is—using the general definition in Ref. [37], p. 27—evaluated as

$$\left\langle J, M_J; 1, 0 | J, 1; J, M_J \right\rangle = M_J \frac{1}{\sqrt{J(J+1)}}, \tag{20}$$

which depends linearly on the total electronic angular momentum projection quantum number M_J. However, the magnetic hyperfine energy must be independent of M_J which is assured by the above prefactor $\frac{1}{M_J}$. Magnetic hyperfine interaction matrix elements have been calculated based on the implementations in references [4,38] which do not make direct use of the Wigner-Eckart theorem and reduced matrix elements.

3. Results and Discussion

3.1. Technical Details

Gaussian atomic basis sets of double-, triple-, and quadruple-ζ quality [39–41] (including correlating functions for $4f$ and $5d$ shells in the case of CI and cvDZ/CC) [42] have been used in the present work.

The atomic spinor basis is obtained in Dirac-Coulomb Hartree–Fock (DCHF) approximation where the Fock operator is defined by averaging over $6p^1_{j=1/2}$ and $6p^1_{j=3/2}$ open-shell electronic configurations.

A locally modified version of the `DIRAC` program package [43] has been used for all electronic-structure calculations. Interelectron correlation effects are taken into account through relativistic Configuration Interaction (CI) theory as implemented in the `KRCI` module [44] of `DIRAC`. Kramer's unrestricted CC calculations have been carried out within the `MRCC` code [45–47]. Both implementations are based on creator-string driven algorithms and can treat expansions of general excitation rank.

The nomenclature for both CI and CC models is defined as: S, D, T, etc. denotes Singles, Doubles, Triples etc. replacements with respect to the reference determinant. The following number is the number of correlated electrons and encodes which occupied shells are included in the CI or CC expansion. In detail we have $3 \mathrel{\widehat{=}} (6s, 6p)$, $13 \mathrel{\widehat{=}} (5d, 6s, 6p)$, $21 \mathrel{\widehat{=}} (5s, 5p, 5d, 6s, 6p)$, $29 \mathrel{\widehat{=}} (4s, 4p, 5s, 5p, 5d, 6s, 6p)$, $31 \mathrel{\widehat{=}} (4d, 5s, 5p, 5d, 6s, 6p)$, $35 \mathrel{\widehat{=}} (4f, 5s, 5p, 5d, 6s, 6p)$. $81 \mathrel{\widehat{=}} (1s, 2s, 2p, 3s, 3p, 3d, 4f, 5s, 5p, 5d, 6s, 6p)$. The notation type S10_SD13, as an example, means that the model SD13 has been approximated by omitting Double excitations from the $(5d)$ shells. CAS3in4 means that an active space is used with all possible determinant occupations distributing the 3 valence electrons over the 4 valence Kramers pairs. Further details about active-space-based correlation expansions are given in Ref. [36].

The use of a Kramer's unrestricted formalism allows performance of coupled cluster calculations of the hyperfine structure constant as well as other properties considered in this paper within the finite-field approach. This method is equivalent to the analytical evaluation of energy derivatives within the Lambda-equation technique [48]. However, some additional uncertainty of the finite-field approach can be expected due to numerical differentiation. To estimate this uncertainty we have compared the values of the effective electric field acting on the electron EDM in Tl placed in the (experimental) external electric field using these two approaches at the CCSD level and cvTZ basis set. The finite-field value differs from the analytical value only by 0.02%. The advantage of the finite-field

approach is that one can use CC models for which the analytical evaluation of energy derivatives is not implemented, in particular in the four-component relativistic domain.

We use the experimental value [49] for the nuclear magnetic moment of ^{205}Tl with nuclear spin $I = \frac{1}{2}$, $\mu = 1.63821[\mu_N]$, in calculations of the magnetic hyperfine interaction constant. In all calculations the Tl nucleus is described by a Gaussian distribution for the nuclear density with exponent taken from Ref. [50].

3.2. Results for Atomic Interaction Constants

The results from the systematic study of many-body effects on atomic EDM enhancement (R), Ne-SPS interaction ratio (S) and magnetic hyperfine interaction constant (A) are compiled in Table 1. The general strategy is to first qualitatively investigate the relative importance of various many-body effects on the properties using a rather small atomic basis set. Then, in a second step, accurate models are developed that include all important many-body effects using the insight from the first step and larger atomic basis sets. Since EDM enhancement and Ne-SPS interaction ratio are analytically related [25] it is sufficient to discuss the trends for R only.

3.3. Step 1: Many-Body Effects in cvDZ Basis

3.3.1. Valence Electron Correlation

The result of $R = -388$ for CAS1in3 which is a singles CI expansion for the electronic ground state can be regarded as close to a DCHF result. The Full CI (FCI) result including only the three valence electrons (CAS3in4_SDT3/60au) of $R = -487$ shows that valence correlation effects lead to a considerable change by more than 25% (in the large cvQZ basis by more than 35%). The valence FCI enhancement in cvQZ basis of $R = -587$ is, therefore, a benchmark. This value is closely reproduced using the universal basis set of reference [22]. Further effects can be considered to be modifications of this benchmark result and will be studied one by one.

3.3.2. Subvalence Electron Correlation

Subvalence electrons of the Tl atoms are those occupying the 5s, 5p, and 5d shells. All other electrons will be considered core electrons. Correlations among the 5d electrons and in particular of the 5d and the valence electrons lead to a strong decrease of R, on the absolute, on the order of 10% (for instance, compare models SD10_CAS3in4_SD13 and CAS3in4_SD3). Corresponding contributions from the 5s and 5p electrons are significantly smaller (compare SD18_CAS3in4_SD21 with SD10_CAS3in4_SD13).

3.3.3. Outer-Core Electron Correlation

Outer-core-valence correlations have been evaluated by allowing for one hole in the respective outer core spinors along with excitations from the subvalence and valence electrons (compare, for instance, S8_SD18_CAS3in4_SDT29 with SD18_CAS3in4_SDT21). In sum for the shells with effective principal quantum number $n = 4$ these effects amount to about 1.5%.

Table 1. R, S, and A for Tl atom. By default, calculations were performed using DCHF spinors for the neutral Tl atom (V^N potential) and, for comparison in selected cases, with the Tl^+ cation (V^{N-1} potential) and Tl^{3+} cation (V^{N-3} potential) spinors.

Model/Virtual Cutoff	***R***	***S* [a.u.]**	$A_{\|\|}$**(^{205}Tl) [MHz]**
Dyall cvDZ			
CAS1in3	−388	269	18,800
CAS3in4	−415	288	18,800
CAS3in4_SD3/60au	−487	339	19,092
CAS3in4_SDT3/60au	−487	339	19,103
S10_CAS3in4_SD13/10au	−458	321	20,003
SD10_CAS3in4_SD13/10au	−442	309	19,502
SD10_CAS3in4_SD13/30au	−441	309	19,575
SD10_CAS3in4_SDT13/10au	−465	326	19,357
SD10_CAS3in4_SDTQ13/10au	−464	326	19,345
SDT10_CAS3in4_SDT13/10au	−460	323	19,254
SDT10_CAS3in4_SDTQ13/10au	−460	323	19,341
SD18_CAS3in4_SD21/10au	−437	307	19,445
SD18_CAS3in4_SD21/10au(Tl^+)	−428	300	18,934
S8_SD18_CAS3in4_SD29/10au	−438	308	19,536
SD18_CAS3in4_SD21/30au	−443	311	19,758
SD18_CAS3in4_SD21/60au	−443	311	19,759
SD8_SD18_CAS3in4_SD29/30au	−449	315	19,980
SD18_CAS3in4_SDT21/10au	−473	331	19,439
SD18_CAS3in4_SDT21/10au(Tl^+)	−467	328	19,228
SDT18_CAS3in4_SDT21/10au	−461	325	19,274
SD18_CAS3in4_SDT21/30au	−483	338	19,761
SD18_CAS3in4_SDT21/60au	−483	338	19,763
S10_SD18_CAS3in4_SDT31/10au	−469	329	19,423
S14_SD18_CAS3in4_SDT35/10au	−469	330	19,448
S8_SD18_CAS3in4_SDT29/30au	−484	340	19,999
SD8_SDT10_CAS3in4_SDT21/10au	−471	331	
SD18_CAS3in4_SDTQ21/10au	−469	329	19,395
Dyall cvTZ			
CAS3in4	−460	323	
CAS3in4_SD3/10au	−565	397	19,027
CAS3in4_SD3/50au	−565	397	19,041
CAS3in4_SDT3/50au	−566	398	19,050
SD18_CAS3in4_SD21/10au	−481	340	19,619
SD18_CAS3in4_SD21/30au	−484	342	19,751
SD18_CAS3in4_SDT21/10au	−542	383	19,995
SD18_CAS3in4_SDT21/10au(Tl^{3+})	−524	371	
SD18_CAS3in4_SDT21/20au	−541	383	
Dyall cvQZ			
CAS1in3	−429	301	18,806
CAS3in4	−476	334	18,806
CAS3in4_SD3/10au	−587	412	19,023
CAS3in4_SD3/35au	−587	412	19,050
CAS3in4_SDT3/35au	−587	413	19,060
SD18_CAS3in4_SD21/35au	−459	322	17,442
SD18_CAS3in4_SDT21/10au	−555	391	20,432
SD18_CAS3in4_SDT21/35au	−562	397	20,592
Nataraj universal			
CAS3in4	−483	339	18,800
CAS3in4_SD3/Nat100	−595	418	19,060
CAS3in4_SD3/200au	−595	418	19,060
SD18_CAS3in4_SD21/45au	−510	361	19,864
cvQZ/SD18_CAS3in4_SDT21/35au + Δ_{corr}	**−539**	**388**	**20,614**

3.3.4. Effect of Higher Excitation Ranks

Allowing for three holes in the shells with effective principal quantum number $n = 5$ and up to four particles in the virtual spinors (*i.e.*, adding combined quadruple excitations) leads to a total change of around 3.5%. Of particular importance are triple excitations into the virtual space, compare models SD18_CAS3in4_SDT21 and SD18_CAS3in4_SD21.

3.4. Step 2: Accurate CI Results

Subsets of important CI models based on the findings of the previous subsection have been repeated using the larger atomic basis sets, cvTZ and cvQZ. The single best values from these calculations are given by the model SD18_CAS3in4_SDT21/35au. These latter values V are then corrected by a "correction shift", calculated as follows (all corrections using cvDZ basis):

$$\begin{aligned}\Delta_{\mathrm{corr}} \;:=\; & V(\mathrm{S10\_SD18\_CAS3in4\_SDT31/10au}) - V(\mathrm{SD18\_CAS3in4\_SDT21/10au}) \\ & + V(\mathrm{S14\_SD18\_CAS3in4\_SDT35/10au}) - V(\mathrm{SD18\_CAS3in4\_SDT21/10au}) \\ & + V(\mathrm{S8\_SD18\_CAS3in4\_SDT29/30au}) - V(\mathrm{SD18\_CAS3in4\_SDT21/30au}) \\ & + V(\mathrm{SDT18\_CAS3in4\_SDT21/10au}) - V(\mathrm{SD18\_CAS3in4\_SDT21/10au}) \\ & + V(\mathrm{SD18\_CAS3in4\_SDTQ21/10au}) - V(\mathrm{SD18\_CAS3in4\_SDT21/10au})\end{aligned}$$

The final best CI values are obtained by adding the above sum of individual corrections to the value from the model SD18_CAS3in4_SDT21/35au.

3.5. Accurate CC Results

Table 2 gives values of R, S and $A_{||}(^{205}\mathrm{Tl})$ constants obtained within the all-electron coupled cluster with single, double and non-iterative triple cluster amplitudes, CCSD(T), method employing several basis sets. One can see a good convergence of the results in the series of the Dyall's DZ, TZ and QZ basis sets: values of R obtained within the QZ and TZ basis sets differ by about 2%. Table 2 also gives values of the constants obtained within the Nataraj's universal basis set [22]. Please note that the latter basis set is the even-tempered basis set (geometry progression). One can see a good agreement of the results obtained within the QZ basis set and Nataraj's universal basis set.

Table 2. R, S, and A for Tl atom calculated within the 81e-CCSD(T) method in different basis sets. In the case denoted "V^N" the atomic spinors are obtained for the neutral Tl atom and the external field perturbs both the spinor coefficients and the CC amplitudes. In the case denoted "V^{N-1}" the atomic spinors are obtained for the Tl^+ cation and the external electric field only perturbs the CC amplitudes but not the atomic spinors.

Basis Set/Virtual Cutoff	***R***	***S* [a.u.]**	$A_{\|\|}(^{205}\mathrm{Tl})$ **[MHz]**
Nataraj universal/10^3au (V^N)	−559	397	21,087
Nataraj universal/10^3au (V^{N-1})	−550	390	21,071
Dyall cvDZ/10^4au (V^N)	−493	347	20,626
Dyall cvTZ/10^4au (V^N)	−545	387	20,760
Dyall cvQZ/10^4au (V^N)	−558	397	21,172

Table 3 gives values of R calculated with different number of correlated electrons. As can be seen contributions from subvalence and outer-core electrons are close to those obtained within the CI approach above.

Table 3. R for Tl atom calculated within the CCSD(T) method in Dyall's cvQZ basis set.

Method/Virtual Cutoff	R
3e-CCSD(T)/10au	−589
21e-CCSD(T)/150au	−527
53e-CCSD(T)/150au	−542
81e-CCSD(T)/10^4au	−558

To check the convergence with respect to electron correlation effects we performed a series of successive 21-electron coupled cluster calculations within the TZ basis set (see Table 4). In these calculations two sets of atomic bispinors were used. The first one was obtained within the DCHF approximation where the Fock operator is defined by averaging over $6p^1_{j=1/2}$ and $6p^1_{j=3/2}$ open-shell electronic configurations as in the CI case above. The second one was obtained within the closed-shell DCHF method for the Tl^+ cation. One can see that CC values gives almost identical result for each set at any level. Moreover, the contribution of correlation effects beyond the CCSD(T) model is almost negligible in the considered case. We considered models up to coupled cluster with Single, Double, Triple and perturbative Quadruple cluster amplitudes, CCSDT(Q).

Contribution of the effect of the Breit interaction on R has been estimated in reference [23] as 0.36%. Based on the uncertainties discussed above we conservatively estimate the uncertainty of our final CC value for R to be less than 5%. For CI the expected residual uncertainties for basis set, inner-core correlations, and inclusion of higher excitation ranks have been added to obtain a final total uncertainty of 6%.

Table 4. Values of R calculated at different level of theory with correlation of 21 electrons of Tl, cvTZ basis set. Calculations were performed using DCHF spinors for the neutral Tl atom (V^N potential) and for the Tl^+ cation (V^{N-1} potential) cases. In both cases the external field perturbs both the spinor coefficients and the CC amplitudes.

	V^N	V^{N-1}
DCHF	−418	−402
CCSD	−531	−530
CCSD(T)	−521	−522
CCSDT	−523	−523
CCSDT(Q)	−522	−522

3.6. Discussion in Comparison with Literature Results

Our present best results are shown in Table 5 in comparison with previous work. The earlier controversy between different groups over results for R(Tl) can be condensed into three main points which we address one by one.

3.6.1. Basis Sets

From the results in Tables 1 and 2 it is evident that a large atomic basis set, at least of quadruple-zeta quality, must be used for obtaining very accurate interaction constants. The results in Tables 1 and 2 obtained with our correlation methods demonstrate that the basis set used by Nataraj et al., in ref. [22] fulfills this requirement, yielding interaction constants that are very close to those obtained with Dyall's cvQZ basis set and the same correlation expansion. The earlier suggestion of Porsev et al., about an inadequate basis set used in ref. [22] can, therefore, be excluded as a possible reason for the outlier result in ref. [22].

Table 5. Comparison with Literature Values.

Work	α_{d_e}	$\alpha_{C_S}[10^{-18}e\ \mathrm{cm}]$	$A_{\|\|}(^{205}\mathrm{Tl})$ [MHz]
Literature values			
Khriplovich et al. [1]		5.1	
Flambaum [51] (semi-empirical)	-500		
Kraftmakher [52] (Hartree–Fock)	-300		
Johnson et al. [26] (Norcross potential)	-562		-18764
Mårtensson–Pendrill et al. [19,53] (estimate)	-600 ± 200	7 ± 2	
Liu et al. [20]	$-585 \pm (30-60)$		
Dzuba et al. [21]	-582 ± 20	7.0 ± 0.2	21067
Nataraj et al., (CCSD(T)) [22]	-466 ± 10		21053
Sahoo et al., (CCSD(T)) [54]		4.06 ± 0.14	21026
Kozlov et al. [55]			21663
Porsev et al. [23]	-573 ± 20		22041
This work CI	-539 ± 33	6.61 ± 0.4	20614
This work CC	-558 ± 28	6.77 ± 0.34	21172
Experiment [56,57]			21310.835 ± 0.005

3.6.2. Treatment of Correlation Effects by the Many-Body Method

It is claimed in reference [22] that the treatment of electron correlation effects was more complete than in references [20,21]. We have therefore first attempted to reproduce the electron EDM enhancement calculated by Nataraj et al., by using the same many-body Hamiltonian and EDM operator, the same atomic basis set ("Nataraj universal") and the same method, CCSD(T). A persisting difference with the approach of Nataraj et al., is the use of CC amplitudes for the closed shells of neutral Tl (our case) or the closed shells of the singly ionized Tl^+ (Nataraj case). These results are shown in Table 2 under the label "V^{N-1}". Our calculation of the hyperfine constant $A_{||} = 21071$ [MHz] reproduces the value of Nataraj et al., which is $A_{||} = 21053$ [MHz] almost precisely (residual difference of less than 0.1%). However, using the same wavefunction we obtain $R = -550$ which differs from the value of Nataraj et al., by 17%. Our CC result for R is in accord with similar calculations using the large cvQZ basis set, in accord with the present best CI result ($R = -539$ which after correction for core correlations from the innermost 28 electrons, according to the results in Table 3, becomes $R = -555$) and in good agreement with the best results of Liu et al., [20], Dzuba et al. [21], and Porsev et al. [23], see Table 5. The correct evaluation of the electron EDM enhancement in our codes has been assured by comparative tests of the independent implementations of present CI and CC, as well as with the `DIRRCI` module [31,58] in the DIRAC program package. All three independent implementations produce the same values of R for small test cases using Full CI/Full CC expansions. These findings strongly suggest that the CC wavefunctions used by us and by Nataraj et al., are almost identical, but that there is a problem in the evaluation of R in reference [22].

Since correlation effects have been treated at a very similar (but physically more accurate) level in the present work as in ref. [22] and the result is very different, the claim of correlation effects being responsible for the large difference between previous results is untenable.

3.6.3. Use of V^N, V^{N-1}, and V^{N-3} Potentials

First, given a fixed atomic basis set and a fixed many-body Hamiltonian (In the present and previous works the Dirac-Coulomb picture is employed where negative-energy states are implicitly or explicitly excluded from the orbital/spinor space which is used as a basis for the many-body expansion.), the Full CI expansion delivers the exact solution in the N-particle sector of Fock space [59], *independent of the orbital/spinor basis used for this Full CI expansion*. This implies that a many-body expansion that closely approximates the Full CI expansion, such as CCSDT or CCSDT(Q), must also be nearly independent of the employed Dirac-Fock potential.

Our results in Table 4 clearly confirm this conjecture and demonstrate that even in the more approximate CCSD expansion the electron EDM enhancement factor R is almost independent (0.2% difference) of the underlying spinor set. As the many-body expansion becomes more approximate, such as in the CI model SD18_CAS3in4_SD21 (see Table 1) basic theory leads us to expect that the difference in R should increase which is indeed the case (roughly 2% difference). Adding external Triple excitations to the CI expansion, model SD18_CAS3in4_SDT21, quenches the difference to a mere 1.2%, again in accord with expectation. Even the use of a V^{N-3} potential (*i.e.*, spinors optimized for the Tl^{3+} system) changes R by less than 3% relative to spinors for the neutral atom in the SD18_CAS3in4_SDT21 model. This difference is expected to be even smaller in CC models.

Despite the unimportance of the employed spinor set in highly correlated calculations, we have used the physically most accurate spinors for the neutral Tl atom in obtaining our best final results. The ratios of our calculated $\mathcal{P},\mathcal{T}$-odd interaction constants are $\left|\frac{\alpha_{d_e}}{\alpha_{C_S}}\right|(\mathrm{CI}) = 81.5\frac{1}{10^{-18}[e\mathrm{cm}]}$ and $\left|\frac{\alpha_{d_e}}{\alpha_{C_S}}\right|(\mathrm{CC}) = 82.6\frac{1}{10^{-18}[e\mathrm{cm}]}$ which agree well with the analytical value of Dzuba et al. [25] of $\left|\frac{\alpha_{d_e}}{\alpha_{C_S}}\right|(\mathrm{an.}) = 89\frac{1}{10^{-18}[e\mathrm{cm}]}$. The validity of this analytical relationship has been confirmed numerically in numerous electronic-structure studies of EDM enhancements and Ne-SPS interactions on other systems, for instance in Refs. [17,18,60–65].

4. Conclusions

In the present study we have carried out a systematic and elaborate treatment of electron correlation effects for the $\mathcal{P},\mathcal{T}$-violating and magnetic hyperfine interaction constants of atomic Tl. This present treatment of electron correlation effects surpasses the one by Nataraj et al., in ref. [22] in that we include higher CC excitation ranks in the wavefunction expansion. Our findings recommend excluding the result of Nataraj et al., from the dataset used to constrain the $\mathcal{CP}$-odd parameters d_e and C_S. Likewise, the result by Sahoo et al. [54] (see Table 5) – presumably obtained with a similar code as R(Tl) by Nataraj et al., – is also to a great degree too small. Our CC ratio for the eEDM and Ne-SPS interaction constants differs from the analytical ratio developed by Dzuba et al. in Refs. [25] by 7.1%. This is within the combined uncertainties of the analytical/numerical approaches used for this comparison. Both the results of Nataraj et al., and Sahoo et al., being too small, the last test is a check for internal consistency of the ratio for those two interaction constants. That ratio amounts to $\left|\frac{\alpha_{d_e}}{\alpha_{C_S}}\right|(\mathrm{CC\ Nataraj/Sahoo}) = 115.8\frac{1}{10^{-18}[e\mathrm{cm}]}$ which deviates from the analytical ratio by 30%, so those two results are even inconsistent with each other.

Figure 2 displays the updated version of the global fit shown in the introduction, using the dataset of reliable calculations of α_{d_e} and α_{C_S} for the Tl atom. The strongly reduced uncertainty of atomic interaction constants for Tl leads to a discernable shrinking of the associated parameter surface (blue), but does not lead to modified constraints. The essential reason for this is the extremely high sensitivity of the experiments on ThO (green) and HfF^+ (orange) and the fact that the surface for Tl is too well aligned with the surfaces for these latter two molecules. However, tighter constraints on d_e and C_S can be obtained by including experimental and theoretical results for closed-shell atomic systems as discussed in ref. [66].

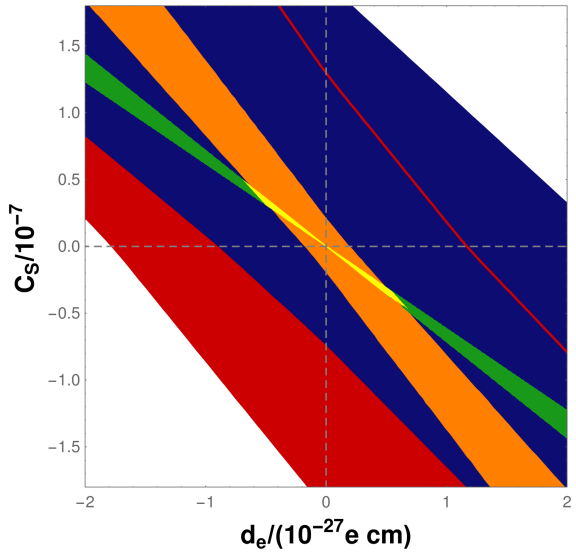

Figure 2. Constraints on d_e and C_S including the results of this work. See text for details.

Author Contributions: Conceptualization, T.F.; Investigation, T.F. and L.V.S.; Methodology, T.F. and L.V.S.; Resources, T.F. and L.V.S.; Software, T.F. and L.V.S.; Writing— original draft, T.F. and L.V.S. All authors have read and agreed to the published version of the manuscript.

Funding: The CC research was funded by Russian Science Foundation Grant No. 19-72-10019.

Acknowledgments: We thank Martin Jung (Torino) for providing updated plots and for helpful discussions. Huliyar Nataraj is thanked for sharing many technical details of his calculations with us. Electronic structure calculations were partially carried out using resources of the collective usage center Modeling and predicting properties of materials at NRC "Kurchatov Institute" – PNPI.

Conflicts of Interest: The authors declare no conflict of interest.

References

1. Khriplovich, I.B.; Lamoreaux, S.K. *CP Violation Without Strangeness*; Springer: Berlin/Heidelberg, Germany, 1997.
2. Engel, J.; Ramsey-Musolf, M.J.; van Kolck, U. Electric dipole moments of nucleons, nuclei, and atoms: The Standard Model and beyond. *Prog. Part. Nuc. Phys.* **2013**, *71*, 21. [CrossRef]
3. Andreev, V.; Hutzler, N.R. Improved limit on the electric dipole moment of the electron. *Nature* **2018**, *562*, 355.
4. Skripnikov, L.V. Combined 4-component and relativistic pseudopotential study of ThO for the electron electric dipole moment search. *J. Chem. Phys.* **2016**, *145*, 214301. [CrossRef]
5. Denis, M.; Fleig, T. In search of discrete symmetry violations beyond the standard model: Thorium monoxide reloaded. *J. Chem. Phys.* **2016**, *145*, 028645. [CrossRef] [PubMed]
6. Cesarotti, C.; Lu, Q.; Nakai, Y.; Parikha, A.; Reece, M. Interpreting the electron EDM constraint. *J. High Energy Phys.* **2019**, *5*, 059. [CrossRef]
7. Dekens, W.; de Vries, J.; Jung, M.; Vos, K.K. The phenomenology of electric dipole moments in models of scalar leptoquarks. *J. High Energy Phys.* **2019**, *069*, 1901. [CrossRef]
8. Chupp, T.; Ramsey-Musolf, M. Electric dipole moments: A global analysis. *Phys. Rev. C* **2015**, *91*, 035502. [CrossRef]
9. Cirigliano, V.; Ramsey-Musolf, M.J.; van Kolck, U. Low energy probes of physics beyond the standard model. *Prog. Part. Nuc. Phys.* **2013**, *71*, 2. [CrossRef]
10. Pospelov, M.; Ritz, A. Electric dipole moments as probes of new physics. *Ann. Phys.* **2005**, *318*, 119. [CrossRef]
11. Barr, S.M. *T*- and *P*-odd electron-nucleon interactions and the electric dipole moments of large atoms. *Phys. Rev. D* **1992**, *45*, 4148. [CrossRef]

12. Kara, D.M.; Smallman, I.J.; Hudson, J.J.; Sauer, B.E.; Tarbutt, M.R.; Hinds, E.A. Measurement of the electron's electric dipole moment using YbF molecules: Methods and data analysis. *New J. Phys.* **2013**, *14*, 103051. [CrossRef]
13. Cairncross, W.B.; Gresh, D.N.; Grau, M.; Cossel, K.C.; Roussy, T.S.; Ni, Y.; Zhou, Y.; Ye, J.; Cornell, E.A. Precision measurement of the electron's electric dipole moment using trapped molecular ions. *Phys. Rev. Lett.* **2017**, *119*, 153001. [CrossRef] [PubMed]
14. Regan, B.C.; Commins, E.D.; Schmidt, C.J.; DeMille, D. New Limit on the Electron Electric Dipole Moment. *Phys. Rev. Lett.* **2002**, *88*, 071805. [CrossRef] [PubMed]
15. Sunaga, A.; Abe, M.; Hada, M.; Das, B.P. Relativistic coupled-cluster calculation of the electron-nucleus scalar-pseudoscalar interaction constant W_S in YbF. *Phys. Rev. A* **2016**, *93*, 042507. [CrossRef]
16. Abe, M.; Gopakumar, G.; Hada, M.; Das, B.P.; Tatewaki, H.; Mukherjee, D. Application of relativistic coupled-cluster theory to the effective electric field in YbF. *Phys. Rev. A* **2014**, *90*, 022501. [CrossRef]
17. Skripnikov, L.V. Communication: Theoretical study of HfF+ cation to search for the T,P-odd interactions. *J. Chem. Phys.* **2017**, *147*, 021101. [CrossRef] [PubMed]
18. Fleig, T. $\mathcal{P},\mathcal{T}$-odd and magnetic hyperfine-interaction constants and excited-state lifetime for HfF^+. *Phys. Rev. A* **2017**, *96*, 040502. [CrossRef]
19. Mårtensson-Pendrill, A.M.; Lindroth, E. Limit on a *P*- and *T*-Violating Electron-Nucleon Interaction. *Eurphys. Lett.* **1991**, *15*, 155. [CrossRef]
20. Liu, Z.W.; Kelly, H.P. Analysis of atomic electric dipole moment in thallium by all-order calculations in many-body perturbation theory. *Phys. Rev. A* **1992**, *45*, R4210. [CrossRef]
21. Dzuba, V.A.; Flambaum, V.V. Calculation of the (T,P)-odd electric dipole moment of thallium and cesium. *Phys. Rev. A* **2009**, *80*, 062509. [CrossRef]
22. Nataraj, H.S.; Sahoo, B.K.; Das, B.P.; Mukherjee, D. Reappraisal of the Electric Dipole Moment Enhancement Factor for Thallium. *Phys. Rev. Lett.* **2011**, *106*, 200403. [CrossRef] [PubMed]
23. Porsev, S.G.; Safronova, M.S.; Kozlov, M.G. Electric Dipole Moment Enhancement Factor of Tl. *Phys. Rev. Lett.* **2012**, *108*, 173001. [CrossRef] [PubMed]
24. Jung, M. A robust limit for the electric dipole moment of the electron. *J. High Energy Phys.* **2013**, *5*, 168. [CrossRef]
25. Dzuba, V.A.; Flambaum, V.V.; Harabati, C. Relations between matrix elements of different weak interactions and interpretation of the parity-nonconserving and electron electric-dipole-moment measurements in atoms and molecules. *Phys. Rev. A* **2011**, *84*, 052108. Erratum ibid, **2012**, 85, 029901. [CrossRef]
26. Johnson, W.R.; Guo, D.S.; Idress, M.; Sapirstein, J. Weak-interaction effects in heavy atomic systems. II. *Phys. Rev. A* **1986**, *34*, 1034. [CrossRef] [PubMed]
27. Commins, E.D. Electric Dipole Moments of Leptons. *Adv. Mol. Opt. Phys.* **1999**, *40*, 1–55.
28. Sushkov, O.P.; Flambaum, V.V.; Khriplovich, I.B. Possibility of investigating *P*- and *T*-odd nuclear forces in atomic and molecular experiments. *Sov. Phys. JETP* **1984**, *60*, 873.
29. Hunter, L.R. Tests of Time-Reversal Invariance in Atoms, Molecules, and the Neutron. *Science* **1991**, *252*, 73. [CrossRef]
30. Lindroth, E.; Lynn, B.W.; Sandars, P.G.H. Order α^2 theory of the atomic electric dipole moment due to an electric dipole moment on the electron. *J. Phys. B* **1989**, *22*, 559. [CrossRef]
31. Fleig, T.; Nayak, M.K. Electron electric-dipole-moment interaction constant for HfF^+ from relativistic correlated all-electron theory. *Phys. Rev. A* **2013**, *88*, 032514. [CrossRef]
32. Skripnikov, L.V.; Maison, D.E.; Mosyagin, N.S. Scalar-pseudoscalar interaction in the francium atom. *Phys. Rev. A* **2017**, *95*, 022507. [CrossRef]
33. Skripnikov, L.V.; Titov, A.V.; Petrov, A.N.; Mosyagin, N.S.; Sushkov, O.P. Enhancement of the electron electric dipole moment in Eu^{2+}. *Phys. Rev. A* **2011**, *84*, 022505. [CrossRef]
34. Flambaum, V.V.; Khriplovich, I.B. New bounds on the electric dipole moment of the electron and on *T*-odd electron-nucleon coupling. *Sov. Phys. JETP* **1985**, *62*, 872.
35. Shukla, A.; Das, B.P.; Andriessen, J. Relativistic many-body calculation of the electric dipole moment of atomic rubidium due to parity and time-reversal violation. *Phys. Rev. A* **1994**, *50*, 1155. [CrossRef] [PubMed]
36. Denis, M.; Nørby, M.; Jensen, H.J.A.; Gomes, A.S.P.; Nayak, M.K.; Knecht, S.; Fleig, T. Theoretical study on ThF^+, a prospective system in search of time-reversal violation. *New J. Phys.* **2015**, *17*, 043005. [CrossRef]

37. Weissbluth, M. *Atoms and Molecules*; Academic Press: New York, NY, USA; San Francisco, CA, USA; London, UK, 1978.
38. Fleig, T.; Nayak, M.K. Electron electric dipole moment and hyperfine interaction constants for ThO. *J. Mol. Spectrosc.* **2014**, *300*, 16. [CrossRef]
39. Dyall, K.G. Relativistic and nonrelativistic finite nucleus optimized double zeta basis sets for the 4p, 5p and 6p elements. *Theoret. Chem. Acc.* **1998**, *99*, 366.
40. Dyall, K.G. Relativistic and nonrelativistic finite nucleus optimized triple-zeta basis sets for the 4p, 5p and 6p elements. *Theoret. Chem. Acc.* **2002**, *108*, 335. [CrossRef]
41. Dyall, K.G. Relativistic double-zeta, triple-zeta, and quadruple-zeta basis sets for the 4p, 5p and 6p elements. *Theoret. Chim. Acta* **2006**, *115*, 441. [CrossRef]
42. Dyall, K.G. Core correlating basis functions for elements 31-118. *Theoret. Chim. Acta* **2012**, *131*, 1217. [CrossRef]
43. Jensen, H.J.A.; Bast, R.; Saue, T.; Visscher, L.; Bakken, V.; Dyall, K.G.; Dubillard, S.; Ekström, U.; Eliav, E.; Enevoldsen, T. DIRAC, a Relativistic ab Initio Electronic Structure Program, Release DIRAC16 (2016). Available online: http://www.diracprogram.org (accessed on 25 February 2020).
44. Knecht, S.; Jensen, H.J.A.; Fleig, T. Large-Scale Parallel Configuration Interaction. II. Two- and four-component double-group general active space implementation with application to BiH. *J. Chem. Phys.* **2010**, *132*, 014108. [CrossRef]
45. Kállay, M.; Rolik, Z.; Ladjánszki, I.; Szegedy, L.; Ladóczki, B.; Csontos, J.; Kornis, B.; Rolik, Z. MRCC, a quantum chemical program suite. *J. Chem. Phys.* **2011**, *135*, 104111. Available online: www.mrcc.hu (accessed on 1 September 2019).
46. Kállay, M.; Surján, P.R. Higher excitations in coupled-cluster theory. *J. Chem. Phys.* **2001**, *115*, 2945–2954. [CrossRef]
47. Kállay, M.; Szalay, P.G.; Surján, P.R. A general state-selective multireference coupled-cluster algorithm. *J. Chem. Phys.* **2002**, *117*, 980–990. [CrossRef]
48. Kállay, M.; Gauss, J.; Szalay, P. Analytic first derivatives for general coupled-cluster and configuration interaction models. *J. Chem. Phys.* **2003**, *119*, 2991.
49. Stone, N.J. (IAEA Nuclear Data Section Vienna International Centre, P.O. Box 100, 1400 Vienna, Austria). *T*able of Nuclear Magnetic Dipole and Electric Quadrupole Moments; INDC International Nuclear Data Committee: Vienna, Austria, 2014.
50. Visscher, L.; Dyall, K.G. Dirac-Fock Atomic Electronic Structure Calculations using Different Nuclear Charge Distributions. *At. Data Nucl. Data Tables* **1997**, *67*, 207. [CrossRef]
51. Flambaum, V.V. To the question of electric-dipole moment enhancement in heavy atoms. *Sov. J. Nucl. Phys.* **1976**, *24*, 199.
52. Kraftmakher, A.Y. On the Hartree-Fock calculation of the electron electric dipole moment enhancement factor for the thallium atom. *J. Phys. B* **1988**, *21*, 2803. [CrossRef]
53. Hartley, A.C.; Lindroth, E.; Mårtensson-Pendrill, A.M. Parity non-conservation and electric dipole moments in caesium and thallium. *J. Phys. B* **1990**, *23*, 3417. [CrossRef]
54. Sahoo, B.K.; Das, B.P.; Chaudhuri, R.; Mukherjee, D.; Venugopal, E.P. Atomic electric-dipole moments from higgs-boson-mediated interactions. *Phys. Rev. A* **2008**, *78*, 010501. [CrossRef]
55. Kozlov, M.G.; Porsev, S.G.; Johnson, W.R. Parity nonconservation in thallium. *Phys. Rev. A* **2001**, *64*, 052107. [CrossRef]
56. Grexa, M.; Hermann, G.; Lasnitschka, G.; Fricke, B. Hyperfine structure and isotopic shift of the n^2P_J levels (n = 7–10) of ^{203,205}Tl measured by Doppler-free two-photon spectroscopy. *Phys. Rev. A* **1998**, *38*, 1263. [CrossRef] [PubMed]
57. Lurio, A.; Prodell, A.G. Hfs Separations and Hfs Anomalies in the $^2P_{\frac{1}{2}}$ state of Ga^{69}, Ga^{71}, Tl^{203} and Tl^{205}. *Phys. Rev.* **1956**, *101*, 79. [CrossRef]
58. Visscher, L.; Saue, T.; Nieuwpoort, W.C.; Fægri, K.; Gropen, O. The electronic structure of the PtH molecule: Fully relativistic configuration interaction calculations of the ground and excited states. *J. Chem. Phys.* **1993**, *99*, 6704. [CrossRef]
59. Helgaker, T.; Jørgensen, P.; Olsen, J. *Molecular Electronic Structure Theory*; John Wiley & Sons: Chichester, UK, 2000.

60. Sasmal, S.; Pathak, H.; Nayak, M.K.; Vaval, N.; Pal, S. Search for parity and time reversal violating effects in HgH: Relativistic coupled-cluster study. *J. Chem. Phys.* **2016**, *144*, 124307. [CrossRef]
61. Sasmal, S.; Talukdar, K.; Nayak, M.K.; Vaval, N.; Pal, S. Electron–nucleus scalar–pseudoscalar interaction in PbF: Z-vector study in the relativistic coupled-cluster framework. *Mol. Phys.* **2017**, *115*, 2807–2812. [CrossRef]
62. Fleig, T. TaO^+ as a candidate molecular ion for searches of physics beyond the standard model. *Phys. Rev. A* **2017**, *95*, 022504. [CrossRef]
63. Gaul, K.; Berger, R. Ab initio study of parity and time-reversal violation in laser-coolable triatomic molecules. *Phys. Rev.* **2018**, *101*, 012508. [CrossRef]
64. Talukdar, K.; Nayak, M.K.; Vaval, N.; Pal, S. Relativistic coupled-cluster investigation of parity (p) and time-reversal (t) symmetry violations in HgF. *J. Chem. Phys.* **2019**, *150*, 084304. [CrossRef]
65. Fazil, N.M.; Prasannaa, V.S.; Latha, K.V.P.; Abe, M.; Das, B.P. RaH as a potential candidate for electron electric-dipole-moment searches. *Phys. Rev. A* **2019**, *99*, 052502. [CrossRef]
66. Fleig, T.; Jung, M. Model-independent determinations of the electron EDM and the role of diamagnetic atoms. *J. High Energy Phys.* **2018**, *7*, 12. [CrossRef]